Macromolecules
ARTICLE

Macromolecules **2010**, *43*, 177–184 **177**
DOI: 10.1021/ma901535p

Kinetic Study of Photoinitiated Frontal Polymerization. Influence of UV Light Intensity Variations on the Conversion Profiles

N. Hayki, L. Lecamp, N. Désilles, and P. Lebaudy*

INSA de Rouen, FRE CNRS 3101, PBS Avenue de l'Université BP 8 76801 Saint Etienne du Rouvray Cedex, France

Received July 15, 2009; Revised Manuscript Received November 6, 2009

ABSTRACT: UV polymerizations in the presence of a photobleachable initiator are studied. The photoinitiator concentration vs time and the UV radiation intensity evolution within the sample are calculated according to rate equations. Polymerization and temperature profiles inside the sample are calculated assuming steady-state conditions. Thermal boundary conditions are chosen for orthopedic applications. The polymerization is then investigated under a range of photoinitiation conditions to access the ability to form thick materials. Theoretical results indicate that both cure depth and temperature rise can be controlled through the use of a photobleachable initiator and variation of the initiating UV radiation intensity during the polymerization.

1. Introduction

Photoinitiated polymerization of multifunctional monomers is one of the most effective methods for producing rapidly three-dimensional polymer networks. The UV curing technology has found a large variety of industrial applications especially in coatings for floor and furniture, dental restorative materials, optical fiber coatings, contact lenses, or photolithography.[1−5]

Light-induced polymerization has several advantages over other methods. In particular, the photochemical process can be performed at low temperature, and the temperature rise resulting from the exothermicity of the reaction can be controlled by changing the irradiation intensity and wavelength. These points are especially important in applications such as orthopedic materials.

The main shortcoming of this process is the limited UV radiation penetration into the material. Indeed, in a classical photoinitiated polymerization process, the incident light is mainly absorbed by the photoinitiator. According to Beer−Lambert's law, this absorption induces a decrease in the UV light intensity in the material thickness. Since the photolysis rate is proportional to the local light intensity, the UV light attenuation leads to a radical concentration gradient in the material. This gradient generally implies a decrease in the polymerization rate and, hence, in the conversion.[6] Consequently, a nonuniform conversion is observed from the top to the bottom of the irradiated material. This incomplete polymerization can dramatically decrease the mechanical properties of the final material, which can then turn inappropriate for numerous applications.

An alternative approach to maintain appropriate polymerization rates and conversions within the material depths is the use of a photobleaching initiator.[7−9] In a photobleaching system, a space−time distribution of light intensity and, hence, of photoinitiator concentration occurs. Indeed, as previously mentioned, light intensity decreases within depth according to Beer−Lambert's law. In addition, in the case of a photobleaching initiator, the photolysis products absorb at a different wavelength from the initiator, leading to a variation of the local UV light intensity with time. Thus, thanks to the medium optical density decrease with irradiation time, UV light can penetrate deeper inside the bulk, allowing the polymerization front to move steadily toward deeper layers. This technique is called frontal polymerization.[10−20]

However, in most cases, either the photobleaching is partial or the polymer (and monomer) absorption cannot be neglected. Hence, an attenuation of the UV light flux can still be observed.[21] The main objective of this work is to show that a thick and homogeneous final material can be obtained while avoiding important temperature rises through variation of the UV radiation intensity during the polymerization.

This work is divided in two parts. The first part deals with computing the photoinitiator decomposition kinetic and its influence on the UV light intensity evolution into the sample. The spatial and temporal light intensity evolution as well as the initiator gradient concentration are described and computed for systems exhibiting either a total or partial photobleaching. Two irradiation modes are applied and discussed: in the first one, the UV light intensity is constant all along the reaction (as it is usually the case), whereas in the second one, a variation of the UV radiation intensity is applied during the reaction in order to keep a homogeneous initiation kinetic inside the material. In the second part of this work, a computational calculation[22−24] based on experimental results and the proportionality relation between UV light intensity[25] and initiation rate is performed. Conversion profiles and temperature distributions inside a thick material are finally obtained as a function of the total, or partial, photobleaching behavior and the irradiation mode.

2. Theoretical Considerations

2.1. Theoretical of a Photobleaching Polymerization. In order to evaluate the photobleaching influence on the UV light penetration into the bulk, a theoretical model is used. In this model, the first step of the photochemical reaction can be described by the following simplified mechanism[26]

$$A \rightarrow B$$

*Corresponding author: Tel +33.2.32.95.65.75; e-mail Philippe.Lebaudy@insa-rouen.fr.

Published on Web 11/17/2009

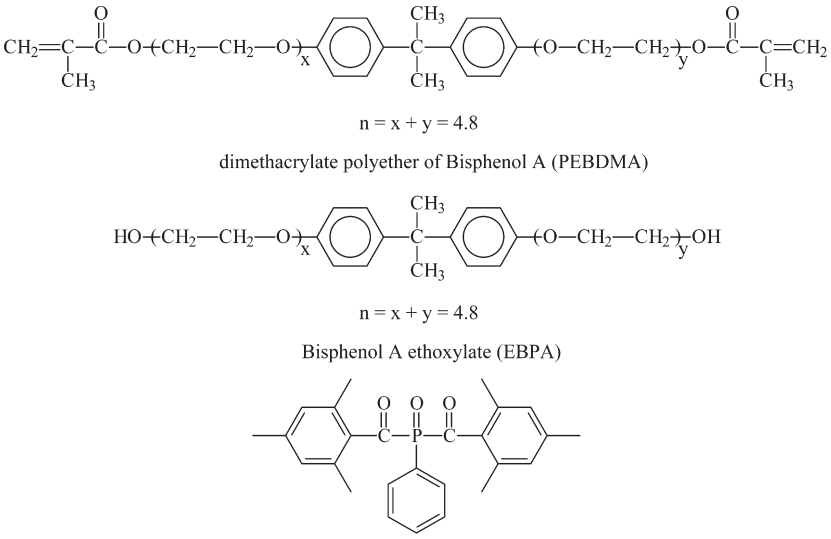

Figure 1. Chemical formula of reactants.

where A represents the photoinitiator characterized by a molar absorption coefficient ε_A and B represents the initiating radical with ε_B as absorption coefficient.

A photobleaching polymerization reaction can be described by this mechanism by choosing adapted values for ε_A and ε_B. If the initiator completely photobleaches, ε_B is equal to zero. For a sample initially homogeneous and subjected to a uniform light normal to the surface, the UV light intensity gradient throughout the sample depth depends on the initiator concentration which itself depends on the sample depth and the reaction time. The following set of coupled partial differential equations describes the initiator concentration and light intensity profiles:

$$-\frac{dC_B(x,t)}{dt} = \frac{dC_A(x,t)}{dt} = -C_A(x,t)\phi I(x,t) \quad (1)$$

$$\frac{dI(x,t)}{dx} = -I(x,t)[\varepsilon_A C_A(x,t) + \varepsilon_B C_B(x,t) + \varepsilon_m C_m(x,t)] \quad (2)$$

$C_A(x,t)$ and $C_B(x,t)$ respectively represent the photoinitiator concentration and the radical concentration at depth x and time t. ϕ is a proportionality coefficient coinciding with the efficient photoinitiator quantum yield. $I(x,t)$ represents the light intensity at depth x and time t. At last, ε_m is the monomer (and the polymer repeating unit) molar absorption coefficient.

If, in addition to a complete initiator photobleaching, the monomer and the polymer repeating unit absorption are negligible, eq is given by

$$\frac{dI(x,t)}{dx} = -I(x,t)\varepsilon_A C_A(x,t) \quad (3)$$

These three coupled differential equations describing the photoinitiator concentration and the light intensity evolutions with time are simultaneously solved by a numerical method with a multiphysics simulation software (Comsol). The following boundaries and initial conditions are applied:

$$dC_A(x,0) = A_0$$
$$dC_B(x,0) = 0$$
$$I(0,t) = I_0$$

2.2. Phenomenological Model for the Photopolymerization Simulation. The simulation developed in this work is based on an autocatalytic kinetic model and describes the photopolymerization rate as a function of temperature, photoinitiator concentration, and light intensity throughout the sample thickness. The complete development of this simulation was described in a previous work.[27]

According to this simulation, the photopolymerization rate can be expressed as follows:

$$\frac{d\chi}{dt} = k\chi^m(\chi' - \chi)^n \quad (4)$$

where n is the reaction order, m is the autocatalytic exponent, k is a rate constant usually assumed to follow an Arrhenius law, and χ' is the ultimate conversion value which is a function of temperature and light intensity.

The energy transport was incorporated into the simulation through an energy balance including heat transfer, heat generation (due to the exothermic nature of the polymerization reaction), and radiation absorption as shown in eq . The absorbing species are primarily the initiator molecules, and the monomer and polymer are considered as transparent in the UV region for a complete photobleaching. The energy balance can be solved as follows:

$$\rho C_p \frac{\partial T}{\partial \tau} = \lambda \frac{\partial^2 T}{\partial x^2} + \Delta H \frac{d\chi}{d\tau} + \varepsilon_A C_A(x,\tau) I(x,\tau) \quad (5)$$

In this equation, ρ and C_p are the density and the specific heat capacity of the polymer, λ is its thermal conductivity, x is the spatial coordinate for sample depth, $d\chi/d\tau$ is the polymerization rate, T is the temperature, τ is the time, $\Delta H(d\chi/d\tau)$ is the location-dependent heat source induced by the polymerization, and ΔH is the photopolymerization enthalpy.

The heat transfer in a polymerizing system is affected by the thermal boundary conditions. Thus, insulating boundary conditions imply a complete retaining of the energy as heat, and conversely, constant temperature boundary conditions imply an almost complete elimination of the heat produced. But, actually, these two boundary conditions are not realistic. That is the reason why the thermal boundary conditions chosen in this work correspond to a bone mold. The theoretical

Scheme 1. Experimental Device for UV-Curing Monitoring: (a) FTIR Setup and (b) Photobleaching Setup

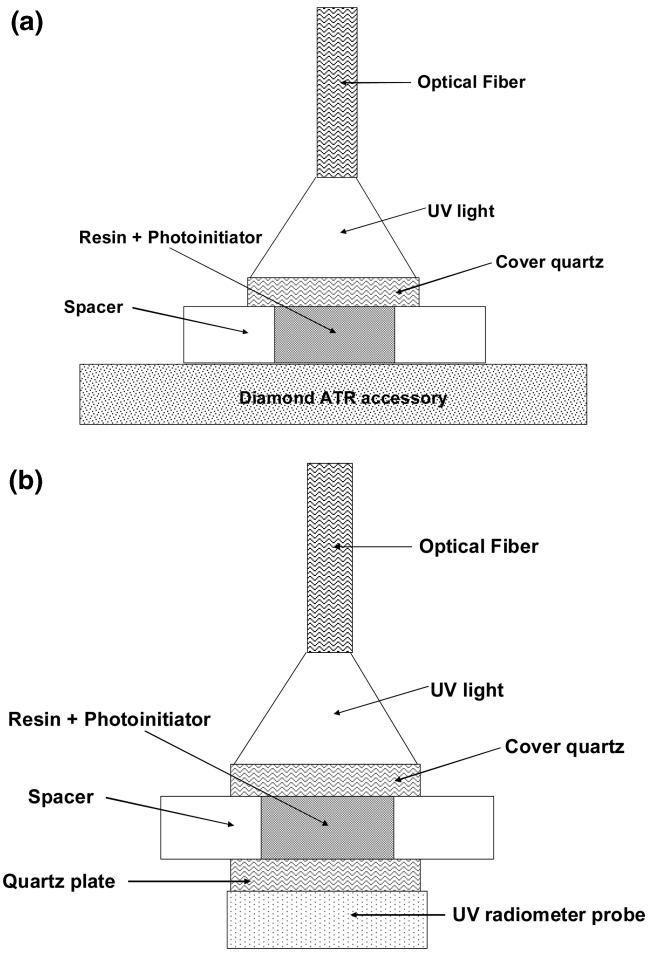

geometry was defined as a 1 cm diameter and 2 cm high cylindrical mold.

As previously mentioned, the two coupled differential equations () and () can be numerically solved by a numerical method using a multiphysics simulation software (Comsol).

3. Experimental Section

3.1. Materials. Figure 1 shows the chemical formulas of the reactants used. Bisphenol A ethoxylate (EBPA) and Bisphenol A ethoxylate dimethacrylate (PEBDMA) were purchased from Aldrich and used without purification. The average number of oxyethyl units is determined by ^{1}H NMR analysis and is equal to 4.8 for the dimethacrylate oligomer (M = 575 g mol^{-1}) and 4.1 for the ethoxylate oligomer (M = 404 g mol^{-1}). The photoinitiator bis(2,4,6-trimethylbenzoyl)phenylphosphine oxide (Irgacure 819, Ciba Geigy Specialties) is dissolved in each oligomer at room temperature under stirring for 3 h with 0.1 and 0.2% (w/w) concentrations.

3.2. Instrumentation and Methods. The photochemical reactions are followed by real-time infrared spectroscopy (Perkin-Elmer FTIR 2000 spectrometer) in attenuated total reflection (ATR). A drop of the reaction mixture is disposed on the ATR and spread out over the ATR diamond crystal with a quartz filter protected by a polyethylene film. The system quartz filter−polyethylene film allows evening out the film and ensuring a constant thickness of the layer. A spacer was applied to observe the thickness effect on the photopolymerization kinetics (Scheme 1a).

The ATR crystal can be set at a chosen temperature by a thermal regulation. The sample is irradiated using a 350 W Oriel mercury vapor lamp. A heat filter is used to reduce sample heating from high irradiation wavelengths. A light guide with a focusing lens is connected to the light source with a fiber-optic cable. The UV radiation intensity is measured at the sample level by a radiometer (VLX-3W Vilber) provided with a probe centered on 365 nm.

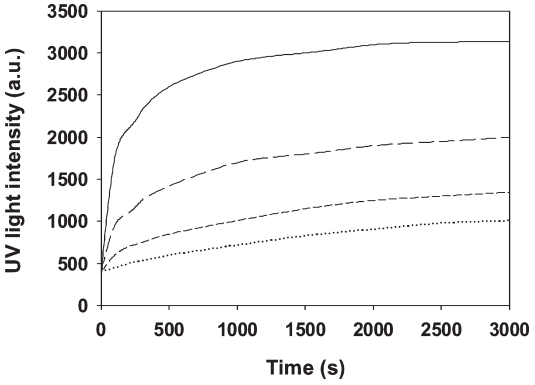

Figure 2. Evolution of the transmitted UV light intensity at 365 nm within 1 mm thick samples for different light intensities irradiation I = 25 mW cm^{-2} (−−−), I = 10 mW cm^{-2} (− − −), I = 5 mW cm^{-2} (---), and I = 1 mW cm^{-2} (···).

The photobleaching kinetics is followed by monitoring the UV light intensity evolution throughout the samples during the photochemical reaction. The samples are located on the UV radiometer probe and irradiated with conditions similar to FTIR experiments (Scheme 1b).

4. Results and Discussion

4.1. Photobleaching Results. The transmitted light flux vs time for 1 mm thick samples, a photoinitiator concentration of 0.1% (w/w), and different UV radiation intensities was experimentally measured (Figure 2). The transmitted light flux evolution is explained by a continuous decrease of the medium optical density with time. The decomposition constant rate of Irgacure 819 is calculated from these results. This evolution is completely independent from the temperature and the nature of the reactant (EBPA and PEBDMA).

From these results, the governing differential equations ()−() were numerically solved. The photobleaching effect is illustrated by curves (Figures 3−6) presenting the light intensity and radical concentration profiles as a function of time and depth in two different cases.

Case 1: Complete Photobleaching (*Theoretical Results*). In this case, the monomer molar absorption coefficient is supposed to be equal to zero (i.e., $\alpha_m = 0$) and the photoinitiator completely bleaches (i.e., $\alpha_A = 0$).

Figure 3a presents the UV light intensity evolution vs depth at different reaction times for a 2 cm thick sample containing 0.1% (w/w) of photoinitiator. At t = 0 (curve in straight line), the light flux penetration in the medium is similar to a non-photobleaching medium: the UV light intensity decreases exponentially in accordance to Beer−Lambert's law. In contrast, when time increases (curves in dotted lines), the light is propagated deeper and deeper through the medium. For an infinite irradiation time, i.e., when the photoinitiator concentration falls to zero, the medium becomes completely transparent and the transmitted light intensity at 2 cm depth is equal to the incident light intensity.

The photoinitiator concentration evolution vs depth and time is shown in Figure 3b. At t = 0 (curve in straight line), this concentration is independent of the sample depth with a normalized value of 1. Then, when time increases (curves in

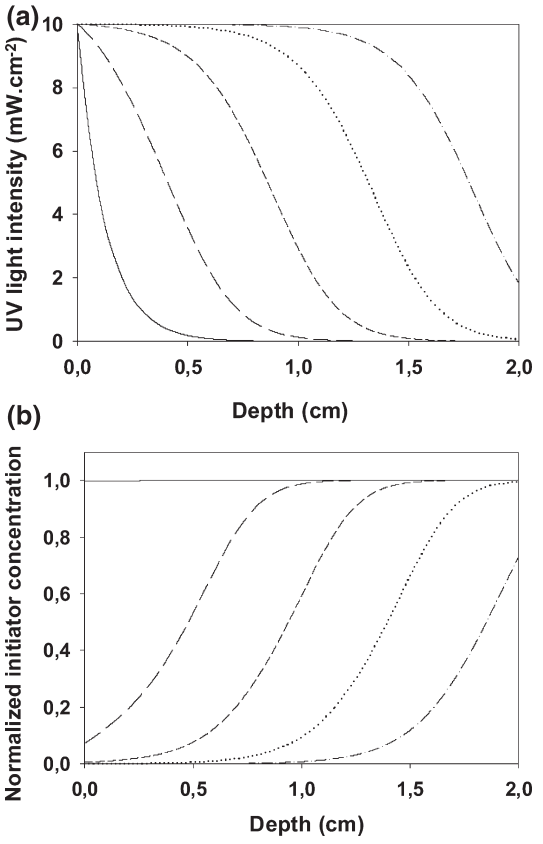

Figure 3. Time and depth dependence of UV light intensity (a) and initiator concentration (b) in a 2 cm thick sample for a total photobleaching and 0.1% (w/w) of photoinitiator. t = 0 s (———), t = 500 s (—— ——), t = 1000 s (— — —), t = 1500 s (· · ·) t = 2000 s (—— · ——), and t = 2500 s (—— ·· ——).

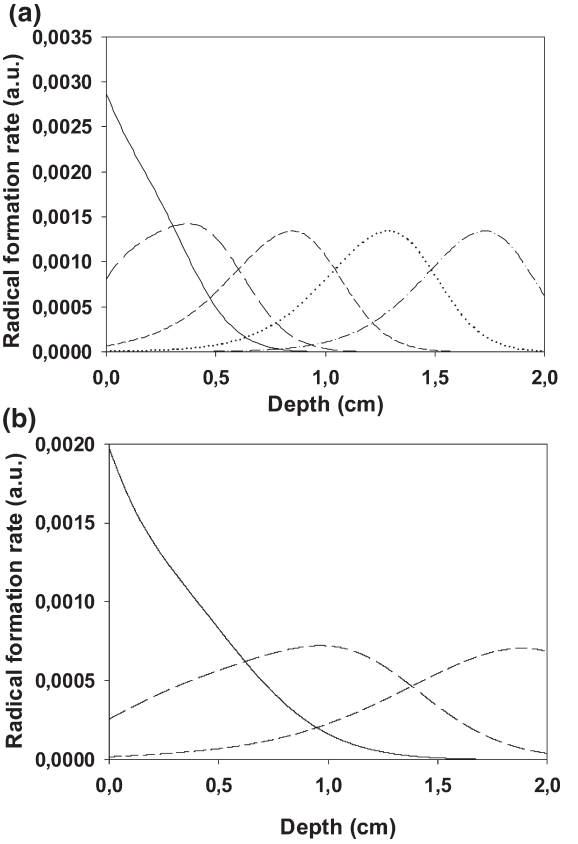

Figure 5. Radical formation rates vs time and depth for a total photobleaching and two photoinitiator concentrations: (a) 0.1% (w/w); (b) 0.05% (w/w). t = 500 s (———), t = 1000 s (—— ——), t = 1500 s (— — —), t = 2000 s (· · ·), t = 2500 s(—— · ——), and t = 3000 s (—— ·· ——).

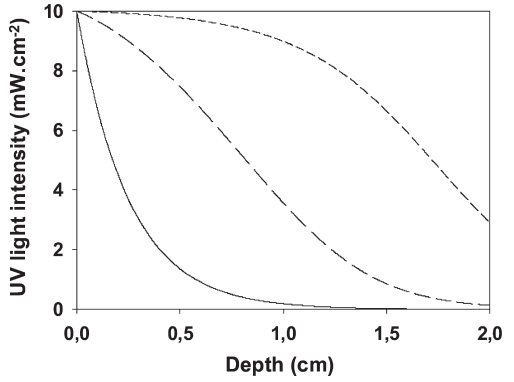

Figure 4. Time and depth dependence of UV light intensity in a 2 cm thick sample for a total photobleaching and a 0.05% (w/w) photoinitiator concentration.

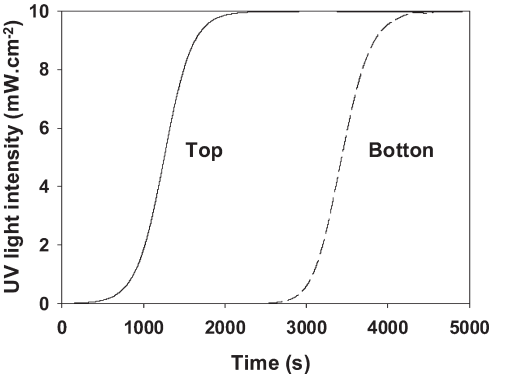

Figure 6. Evolution of the UV light intensity at the top and the bottom of the sample for a total photobleaching and a photoinitiator concentration of 0.1% (w/w).

dotted lines), the photoinitiator is consumed at a rate proportional to the local UV light intensity. Consequently, the fastest initiator concentration decrease is localized near the illuminated surface. This results in a transmittance increase near the surface. The initiator concentration evolution presents a sigmoid shape with a nearly zero concentration near the irradiated surface. The region with a nearly zero initiator concentration expands as the system bleaches. For an infinite irradiation time, the photoinitiator has completely reacted in the overall material.

Figure 4 shows the transmitted light intensity evolution as a function of depth and time for a photoinitiator concentration reduced by half. This profile illustrates a faster photobleaching process when using a lower initial initiator concentration.

The profiles of radical formation rates vs depth for different reaction times and photoinitiator concentrations (Figure 5) illustrate some interesting trends that can be discussed. First, the radical formation rate is not uniform but significantly varies with time and depth within the sample. Thus, the radical formation rate evolution curve at a given time presents a maximum at a x_m depth. For depths lower than x_m, the rate progressively decreases when approaching the illuminated surface because the initiator has been more and more depleted in this region. Then, for depths higher than x_m, the rate decreases because of the light

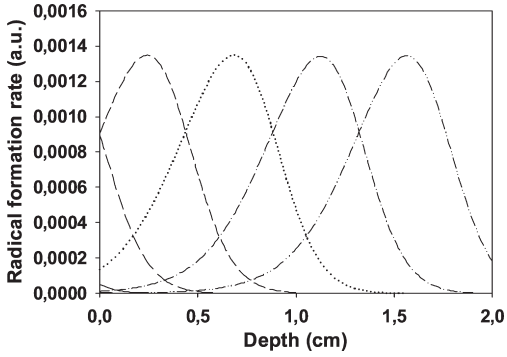

Figure 7. Radical formation rates vs depth and reaction time for a total photobleaching and for the variable light intensity depicted in Figure 6. t = 500 s (−−−), t = 1000 s (−− −−), t = 1500 s (− − −), t = 2000 s (···), t = 2500 s (−− · −−), and t = 3000 s (−− ·· −−).

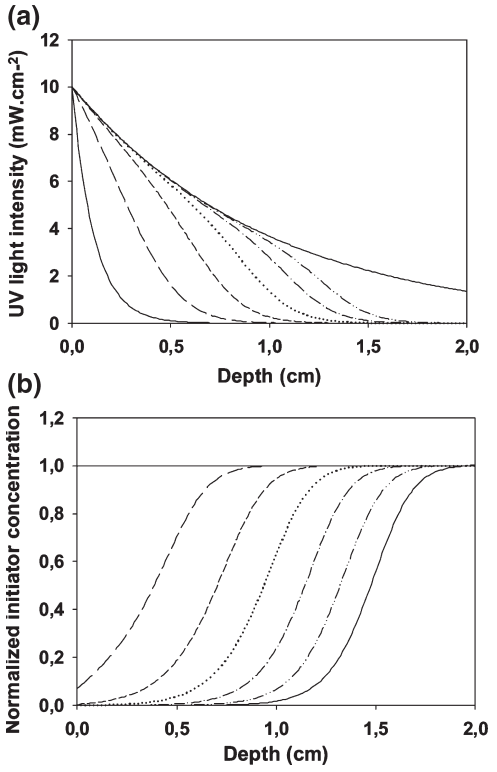

Figure 8. Time and depth dependence of light intensity (a) and initiator concentration (b) in a 2 cm thick sample for a partial photobleaching and a 0.1% (w/w) photoinitiator concentration. t = 0 s (−−−), t = 500 s (−− −−), t = 1000 s (− − −), t = 1500 s (···), t = 2000 s (−− · −−), and t = 2500 s (−− ·· −−).

intensity reduction. Therefore, at any given time, the radical formation rate profile looks like a wavefront. This type of wave propagation is well-known in the literature.[28,29]

Second, the radical formation rate is maximum for a highest initiator concentration as shown by comparison of Figure 5a,b. For a higher initiator concentration, the UV light depth penetration and the spatial propagation of the radical formation rate wave are restricted. On the contrary, a lower initiator concentration allows an efficient penetration of the UV light into the sample but the radical formation rate is lower. Finally, the radical formation rate exhibits a maximum at the sample surface independently of the initiator concentration. This maximum arises from the difference between the temporal variations of the UV intensity at the surface and inside the sample. Indeed, the UV intensity

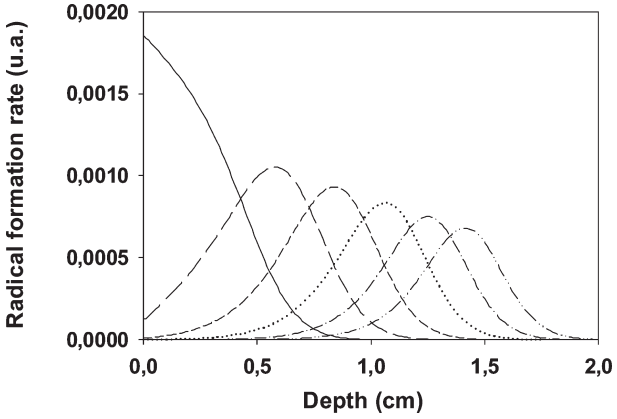

Figure 9. Radical formation rates vs time for a partial photobleaching and a photoinitiator concentration of 0.1% (w/w). t = 500 s (−−−), t = 1000 s (−− −−), t = 1500 s (− − −), t = 2000 s (···), t = 2500 s (−− · −−), and t = 3000 s (−− ·· −−).

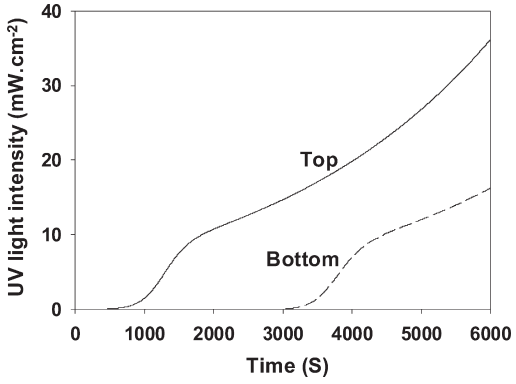

Figure 10. Evolution of the UV light intensity at the top and the bottom of the sample for a partial photobleaching and a photoinitiator concentration of 0.1% (w/w).

instantaneously increases from 0 to 10 mW cm^{-2} at the sample surface, whereas a sigmoid variation of the UV intensity is observed inside the sample in accordance with the initiator concentration evolution.

Hence, a homogeneously polymerization will be observed if a homogeneous radical formation rate profile can be obtained throughout the sample. In this aim, a sigmoid variation of the UV light intensity was imposed at the sample surface (Figure 6). With these lighting conditions, the radical formation rate is the same in the overall sample depth as plotted in Figure 7.

Case 2: Partial Photobleaching (*Theoretical Results*). Figure 8a presents the UV light intensity evolution vs depth for different reaction times in the case of a 2 cm thick sample containing 0.1% (w/w) of photoinitiator and with a partial photobleaching (i.e., $\varepsilon_B \neq 0$) or a nonnegligible polymer absorption (i.e., $\varepsilon_m \neq 0$). An attenuation of the light intensity is clearly observed.

Figure 8b shows the collateral evolution of the photoinitiator concentration as a function of depth and time. By comparison with Figure 3b (total photobleaching), we clearly observe that the light intensity attenuation significantly decreases the spatial propagation rate throughout the sample.

The radical formation rate as vs depth profiles are presented in Figure 9 for different reaction times. Globally, the curve shape is similar to Figure 5. The difference lies in the decreases, on one hand, of the radical formation maximum rate and, on the other hand, of the wavefront propagation

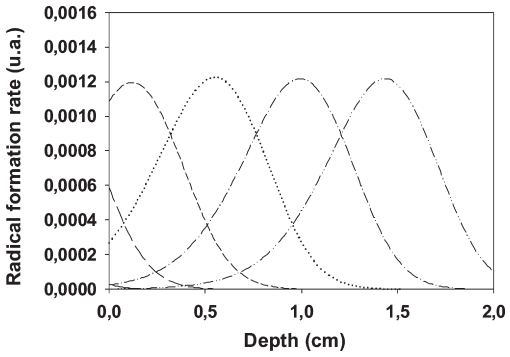

Figure 11. Radical formation rates vs depth and reaction time for a partial photobleaching and for the variable light intensity depicted in Figure 10. t = 500 s (———), t = 1000 s (—— ——), t = 1500 s (— — —), t = 2000 s (···), t = 2500 s (—— · ——), and t = 3000 s (—— ·· ——).

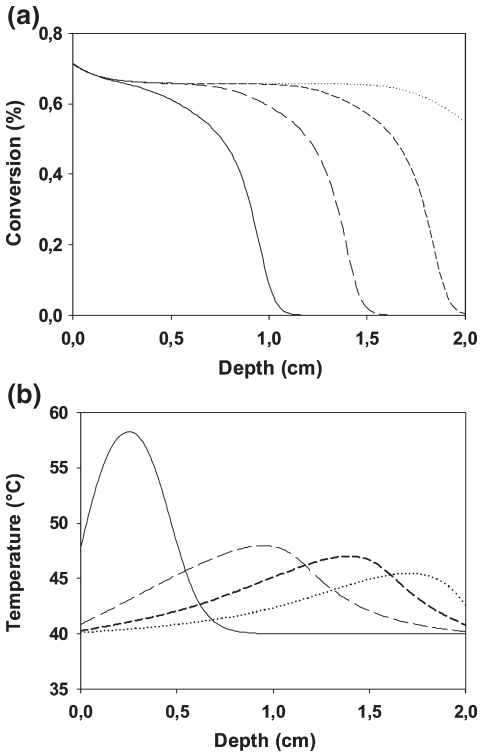

Figure 12. Conversion (a) and temperature (b) evolutions vs depth and reaction time in a 2 cm thick sample for a total photobleaching and 0.1% (w/w) of photoinitiator. t = 500 s (———), t = 1000 s (—— ——), t = 1500 s (— — —), t = 2000 s (···), t = 2500 s (—— · ——), and t = 3000 s (—— ·· ——).

rate. These decreases, explained by the UV light intensity reduction through the sample depth, lead to a nonuniform photopolymerization.

Besides the sigmoid variation of the UV light intensity which has been previously applied, an exponential variation vs time should be applied to compensate the UV intensity decrease due to the polymer absorption (Figure 10). With these lighting conditions, the radical formation rate is homogeneous throughout the sample depth (Figure 11).

4.2. Photopolymerization Theoretical Results. Conversion kinetics and temperature evolution were experimentally measured on thin samples (i.e., in isothermal conditions and with a uniform irradiation).[30] The samples were UV-cured under a monochromatic radiation at 365 nm for different incident light intensity values (1 to 100 mW cm^{-2}). Thanks to the differential eq in which m and n have been

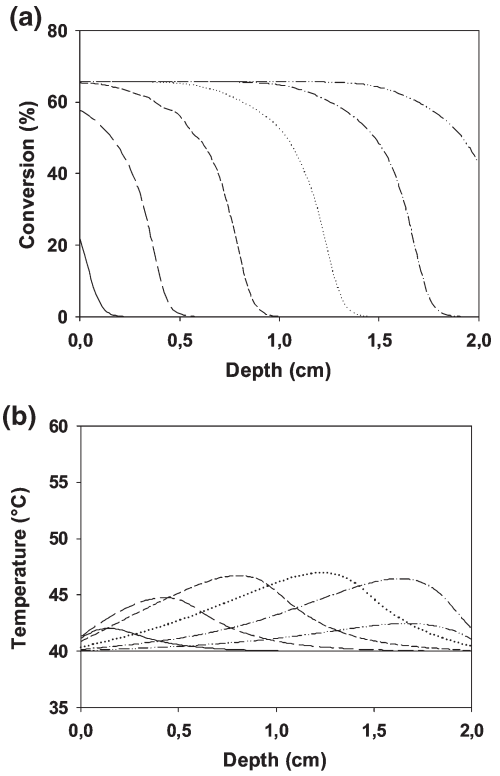

Figure 13. Conversion (a) and temperature (b) evolutions vs depth and reaction time in a 2 cm thick sample for a total photobleaching, 0.1% (w/w) of photoinitiator, and the variable light intensity depicted in Figure 6. t = 500 s (———), t = 1000 s (—— ——), t = 1500 s (— — —), t = 2000 s (···), t = 2500 s (—— · ——), and t = 3000 s (—— ·· ——).

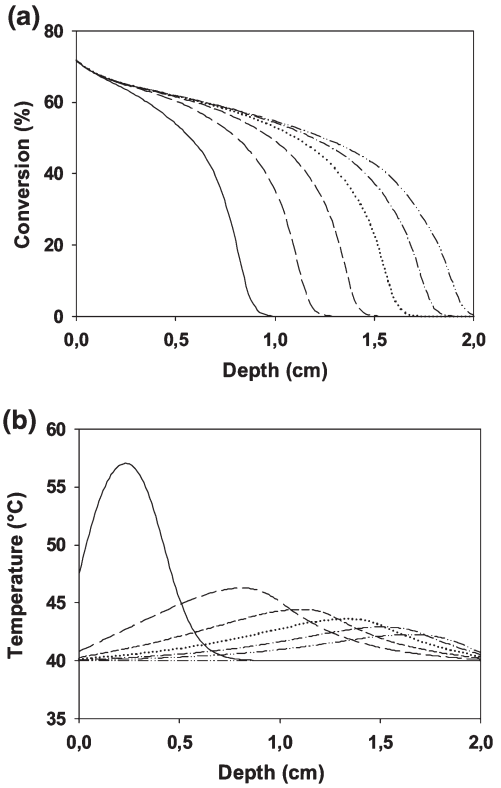

Figure 14. Conversion (a) and temperature (b) profiles versus depth and reaction time in a 2 cm thick sample for a partial photobleaching and 0.1% (w/w) of photoinitiator. t = 500 s (———), t = 1000 s (—— ——), t = 1500 s (— — —), t = 2000 s (···), t = 2500 s (—— · ——), and t = 3000 s (—— ·· ——).

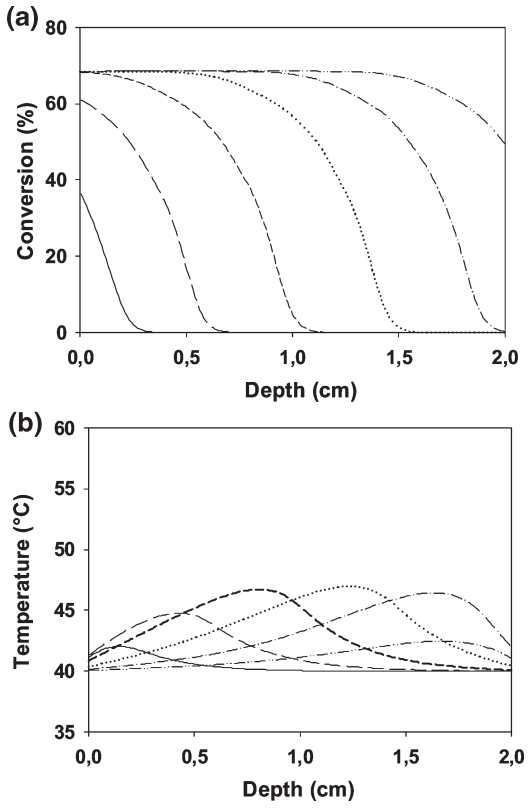

Figure 15. Conversion (a) and temperature (b) profiles vs depth and reaction time in a 2 cm thick sample for a partial photobleaching, 0.1% (w/w) of photoinitiator, and the variable light intensity depicted in Figure 10. t = 500 s (———), t = 1000 s (— — —), t = 1500 s (— — —), t = 2000 s (· · ·), t = 2500 s (— · —), and t = 3000 s (— · · —).

determined to be equal to 0.8 and 2, respectively,[27] k and χ' are now calculated from the aforementioned experimental kinetic results. Then, by interpolation, the evolution of the conversion χ can be described versus time, temperature, and intensity.[31]

Knowing the photoinitiation rate and the conversion kinetic parameters, the conversion and temperature profiles in the bulk can be computed. The simulation is based on the proven finite elements method.

Case 1: Total Photobleaching. Figure 12 presents the conversion and temperature evolutions as a function of depth and time for conditions similar to those used in Figure 3 (i.e., total photobleaching and I_0 = 10 mW cm^{-2}). Except for the surface, the ultimate conversion is homogeneous inside the sample (Figure 12a). On the surface, the higher conversion is related to the radical formation rate which exhibits a maximum on this location and to the temperature (Figure 12b) which tends to increase due to the higher reaction rate.

Figure 13 presents the conversion and temperature profiles as a function of depth and time for the lighting conditions of Figure 6 (sigmoid variation of the UV light intensity). As expected, the conversion begins slower. The ultimate conversion is homogeneous in all the material thickness (Figure 13a), and the temperature does not present a maximum on the surface and does not exceed 47 °C (Figure 13b).

Case 2: Partial Photobleaching. Figure 14 presents the conversion and temperature profiles as a function of depth and time for conditions similar to Figure 8 (i.e., partial photobleaching and I_0 = 10 mW cm^{-2}). At the sample surface, the results are similar to those of Figure 12a. In contrast, when the thickness increases, the conversion falls because of the UV radiation intensity decrease (Figure 14a). The ultimate conversion is not homogeneous inside the sample, and the temperature presents a maximum on the surface because of the reaction rate (Figure 14b).

Figure 15 presents the conversion and temperature profiles as a function of depth and time for conditions similar to Figure 11 (i.e., partial photobleaching, sigmoid and exponential variation of the UV light intensity). The conversion begins slowly as in Figure 13, and the ultimate conversion is homogeneous in all the material thickness (Figure 15a). The temperature profile is also homogeneous throughout the sample and does not exceed 47 °C (Figure 15b).

5. Conclusions

In this contribution, numerical calculations were conducted to describe the spatial and temporal evolution of transmitted UV light intensity, initiator concentration, radical formation rate, conversion profiles, and temperature evolution for total or partial photobleaching systems. Simulation results showed that, at any given time, the radical formation rate profile is a wavefront. The breadth of this wavefront is determined by the initial initiator concentration and the material absorption. The highest radical formation rate at the wavefront peak is obtained with a high initiator concentration, but in this case, the UV light penetration depth and the spatial propagation of the radical formation rate wave are restricted. A lower initiator concentration allows an efficient penetration of the UV light into the sample, but the radical formation rate is decreased.

These simulation results also illustrate that, for the UV curing of thick systems exhibiting a partial photobleaching, a homogeneous polymerization can be obtained through a sigmoid increase in the UV light intensity during the polymerization. Moreover, the ultimate conversion may significantly change if any variable of the system is changed, i.e., UV light intensity, monomer, initiator, and photobleaching degree.

Finally, this simulation can be applied to any combination of monomer, initiator, and light source as long as the physicochemical properties of the studied system are known. This numerical calculation may provide an interesting tool to optimize the selection of the initial products and to understand these effects on the final conversion.

References and Notes

(1) Finter, J.; Frischinger, I.; Haug, T.; Marton, R. RadTech Europe Conference Proc, 489, Lyon, France, **1997**.
(2) Anseth, K. S.; Newman, S. N.; Bowman, C. N. *Adv. Polym. Sci.* **1995**, 122–177.
(3) Abadie, M. J. M.; Parfait, A.; Rouby, M. *Eur. Polym. J.* **1994**, 30–399.
(4) Cook, W. D. *J. Macromol. Sci., Chem.* **1982**, 17–99.
(5) Cook, W. D. *Polymer* **1992**, *33*, 600–609.
(6) Désilles, N.; Lecamp, L.; Lebaudy, P.; Bunel, C. *Polymer* **2003**, *44*, 6159–6167.
(7) Asmussen, S.; Arenas, G.; Cook, W.; Vallo, C. *Eur. Polym. J.* **2009**, 515–522.
(8) Yang, Y. C.; Zeng, Z.; Zeng, Z.; Chen, Y. *Polymer* **2007**, *43*, 3912–3922.
(9) Cabral, J. T.; Douglas, J. F. *Polymer* **2005**, *46*, 4230–4241.
(10) Ivanov, V.; Decker, C. *Polym. Int.* **2001**, *50*, 113–118.
(11) Briskman, V. A.; Kostarev, K. G.; Levtov, V.; Lyubimova, T.; Mashinsky, A.; Nechitailo, G.; Romanov, V. *Acta Astronaut.* **1996**, *39*, 395–402.
(12) Belk, M.; Kostarev, K. G.; Volpert, V.; Yudina, T. M. *J. Phys. Chem. B* **2003**, *107*, 10292–10298.
(13) Cabral, J. T.; Hudson, S. D.; Harrison, C.; Douglas, J. F. *Langmuir* **2004**, *20*, 10020–10029.
(14) Decker, C.; Keller, L.; Zahouily, K.; Benfarhi, S. *Polymer* **2005**, *46*, 6640–6648.

(15) Warren, J. A.; Cabral, J. T.; Douglas, J. F. *Phys. Rev. E* **2005**, *72*, 021801.
(16) Tao, Y.; Yang, J.; Zeng, Z.; Chen, Y. *Polym. Int.* **2006**, *55*, 418–425.
(17) Cui, Y.; Yang, J.; Zeng, Z.; Chen, Y. *Eur. Polym. J.* **2007**, *43*, 3912–3922.
(18) Cui, Y.; Yang, J.; Zeng, Z.; Chen, Y. *Polymer* **2007**, *48*, 5994–6001.
(19) Cui, Y.; Yang, J.; Zhan, Y.; Zeng, Z.; Chen, Y. *Colloid Polym. Sci.* **2008**, *286*, 97–106.
(20) Kostarev, K. G.; Svistkov, A. L.; Shmyrov, A. V. *Polym. Sci., Ser. A* 20.
(21) Johnson, P. M.; Stansbury, J. W.; Bowman, C. N. *Polymer* **2007**, *48*, 6319–6324.
(22) Lecamp, L.; Lebaudy, P.; Youssef, B.; Bunel, C. *Polymer* **2001**, *42*, 8541–8547.
(23) Azan, V.; Lecamp, L.; Lebaudy, P.; Bunel, C. *Prog. Org. Coat.* **2007**, *58*, 70–75.
(24) Désilles, N.; Lecamp, L.; Lebaudy, P.; Youssef, B.; Lebaudy, Z.; Bunel, C. *Polymer* **2006**, *47*, 193–199.
(25) Lecamp, L.; Youssef, B.; Bunel, C.; Lebaudy, P. *Polymer* **1997**, *38*, 6089–6096.
(26) Bityurin, N.; Pikulin, A.; Alexandrov, A. *Appl. Surf. Sci.* **2003**, *208−209*, 481–485.
(27) Lecamp, L.; Youssef, B.; Bunel, C.; Lebaudy, P. *Polymer* **1999**, *40*, 1403–1409.
(28) Miller, G.; Gou, L.; Narayanan, V.; Scranton, B. *J. Polym. Sci., Part A* **2002**, *40*, 793–808.
(29) Terrones, G.; Pearlstein, A. *Macromolecules* **2001**, *34*, 3195–3204.
(30) Lecamp, L.; Lebaudy, P.; Youssef, B.; Bunel, C. *J. Therm. Anal.* **1998**, *51*, 889–895.
(31) Lecamp, L.; Lebaudy, P.; Youssef, B.; Bunel, C. *Macromol. Symp.* **1999**, *148*, 77–86.